# A local discontinuous Galerkin method for the Camassa-Holm equation

Yan Xu[*] and Chi-Wang Shu [†]

January 10, 2007

## Abstract

In this paper, we develop, analyze and test a local discontinuous Galerkin (LDG) method for solving the Camassa-Holm equation which contains nonlinear high order derivatives. The LDG method has the flexibility for arbitrary $h$ and $p$ adaptivity. We prove the $L^2$ stability for general solutions and give a detailed error estimate for smooth solutions, and provide numerical simulation results for different types of solutions of the nonlinear Camassa-Holm equation to illustrate the accuracy and capability of the LDG method.

**AMS subject classification: 65M60, 35Q53**

**Key words:** local discontinuous Galerkin method, Camassa-Holm equation, stability, error estimate

# 1   Introduction

In this paper, we consider numerical approximations to the Camassa-Holm (CH) equation [4, 5]

$$u_t - u_{xxt} + 2\kappa u_x + 3uu_x = 2u_x u_{xx} + uu_{xxx}, \tag{1.1}$$

where $\kappa$ is a constant. Such nonlinearly dispersive partial differential equations support peakon solutions. The lack of smoothness at the peak of the peakon introduces high-frequency dispersive errors into the calculation. It is a challenge to design stable and accurate numerical schemes for solving this equation.

We develop a class of local discontinuous Galerkin (LDG) methods for this nonlinear CH equation. Our proposed scheme is high order accurate, nonlinear stable and flexible

---

[*]Department of Applied Mathematics, University of Twente, P.O. Box 217, 7500 AE, Enschede, The Netherlands. E-mail: y.xu@math.utwente.nl

[†]Division of Applied Mathematics, Brown University, Providence, RI 02912, USA. E-mail: shu@dam.brown.edu. Research supported by ARO grant W911NF-04-1-0291 and NSF grant DMS-0510345.

# Report Documentation Page

Public reporting burden for the collection of information is estimated to average 1 hour per response, including the time for reviewing instructions, searching existing data sources, gathering and maintaining the data needed, and completing and reviewing the collection of information. Send comments regarding this burden estimate or any other aspect of this collection of information, including suggestions for reducing this burden, to Washington Headquarters Services, Directorate for Information Operations and Reports, 1215 Jefferson Davis Highway, Suite 1204, Arlington VA 22202-4302. Respondents should be aware that notwithstanding any other provision of law, no person shall be subject to a penalty for failing to comply with a collection of information if it does not display a currently valid OMB control number.

| 1. REPORT DATE **10 JAN 2007** | 2. REPORT TYPE | 3. DATES COVERED **00-00-2007 to 00-00-2007** |
|---|---|---|

| 4. TITLE AND SUBTITLE **A local discontinuous Galerkin method for the Camassa-Holm equation** | 5a. CONTRACT NUMBER |
|---|---|
| | 5b. GRANT NUMBER |
| | 5c. PROGRAM ELEMENT NUMBER |
| 6. AUTHOR(S) | 5d. PROJECT NUMBER |
| | 5e. TASK NUMBER |
| | 5f. WORK UNIT NUMBER |
| 7. PERFORMING ORGANIZATION NAME(S) AND ADDRESS(ES) **Brown University,Division of Applied Mathematics,182 George Street,Providence ,RI,02192** | 8. PERFORMING ORGANIZATION REPORT NUMBER |
| 9. SPONSORING/MONITORING AGENCY NAME(S) AND ADDRESS(ES) | 10. SPONSOR/MONITOR'S ACRONYM(S) |
| | 11. SPONSOR/MONITOR'S REPORT NUMBER(S) |

12. DISTRIBUTION/AVAILABILITY STATEMENT
**Approved for public release; distribution unlimited**

13. SUPPLEMENTARY NOTES

14. ABSTRACT

15. SUBJECT TERMS

| 16. SECURITY CLASSIFICATION OF: | | | 17. LIMITATION OF ABSTRACT | 18. NUMBER OF PAGES **28** | 19a. NAME OF RESPONSIBLE PERSON |
|---|---|---|---|---|---|
| a. REPORT **unclassified** | b. ABSTRACT **unclassified** | c. THIS PAGE **unclassified** | | | |

for arbitrary $h$ and $p$ adaptivity. The proof of the $L^2$ stability of the scheme is given for general solutions. Error estimates are given for smooth solutions. To our best knowledge, this is the first provably stable finite element method for the Camassa-Holm equation.

The main motivation for the algorithm discussed in this paper originates from the LDG techniques which have been developed for convection diffusion equations (containing second derivatives) [9] and nonlinear wave equations with high order derivatives [32, 33, 24, 27, 28, 29, 30]. In these papers, stable LDG method for quite general nonlinear wave equations including multi-dimensional and system cases have been developed. The proof of the nonlinear $L^2$ stability of these methods are usually given and successful numerical experiments demonstrate their capability. These results indicate that the LDG method is a good tool for solving nonlinear equations in mathematical physics.

There are only a few works in the literature for error estimates of the LDG method for nonlinear wave equations with high order derivatives. In [31], *a priori* error estimates are given for the LDG method for nonlinear convection-diffusion equations and KdV equations. There are technical difficulties to derive the $L^2$ *a priori* error estimates from the cell entropy inequality and approximation results, because of the possible lack of control on some of the jump terms at cell boundaries, which appear because of the discontinuous nature of the finite element space for the DG method. The remedy in [31] to handle such jump terms is via a special projection, which eliminates such troublesome jump terms in the error equation. It is more challenging to perform $L^2$ *a priori* error estimates for nonlinear PDEs with high order derivatives than for first order hyperbolic PDEs in [34].

The CH equation (1.1) was derived as a model for the propagation of the unidirectional gravitational waves in a shallow water approximation, with $u$ representing the free surface of water over a flat bed [4, 5, 18]. The CH equation has a very intriguing structure. For instance, it is completely integrable and models wave breaking for a large class of initial data. This equation has attracted a lot of attention in the literature. Lenells gave a detailed discussion of its conservation law in [23] and also classified all the weak traveling wave solutions in [22]. Johnson [19] implemented the inverse-scattering transform method to the solution of the CH equation. Li and Zhang [25] used the same method to solve a multiple-soliton for the CH equation. Bressan and Constantin [2, 3] developed a new approach for its analysis, particularly for the investigation of the wave breaking.

There are only a few numerical works in the literature to solve the CH equation. Holden and Raynaud [17] proved the convergence of a finite difference method for the CH equation and they also developed a convergent numerical scheme based on multipeakon in [16]. Several different aspects of periodic traveling wave solutions of the CH equation were numerically explored in [20] and the error analysis of a spectral projection of the periodic CH equation was given in [21]. A finite-volume method was developed in [1] to simulate the dynamics of peakons.

The discontinuous Galerkin (DG) method we discuss in this paper is a class of finite element methods using completely discontinuous piecewise polynomial space for the nu-

merical solution and the test functions in the spatial variables. The DG discretization results in an extremely local, element based discretization, which is beneficial for parallel computing and maintaining high order accuracy on unstructured meshes. In particular, DG methods are well suited for $hp$-adaptation, which consists of local mesh refinement and/or the adjustment of the polynomial order in individual elements. They also have excellent provable nonlinear stability. The LDG method for the Camassa-Holm equation (1.1) that we design in this paper shares all these nice properties. More general information about DG methods can be found in [7, 10, 11, 12]. Recently, Eskilsson and Sherwin [13, 14, 15] also presented discontinuous spectral element methods for simulating 1D linear Boussinesq-type equations, dispersive shallow water systems and 2D Boussinesq equations.

The paper is organized as follows. In Section 2, we present and analyze our LDG method for the Camassa-Holm equation (1.1). In Section 2.2, we present the LDG method. Details related to the implementation of the method are described in Section 2.3. We give a proof of the $L^2$ stability in Section 3, and present an *a priori* error estimate in Section 4. Section 5 contains numerical results to demonstrate the accuracy and capability of the methods. Concluding remarks are given in Section 6. Some of the more technical proofs of several lemmas are collected in the Appendix.

# 2    The LDG method for the Camassa-Holm equation

## 2.1    Notation

We denote the mesh by $I_j = [x_{j-\frac{1}{2}}, x_{j+\frac{1}{2}}]$, for $j = 1, \ldots, N$. The center of the cell is $x_j = \frac{1}{2}(x_{j-\frac{1}{2}} + x_{j+\frac{1}{2}})$ and the mesh size is denoted by $h_j = x_{j+\frac{1}{2}} - x_{j-\frac{1}{2}}$, with $h = \max_{1 \leq j \leq N} h_j$ being the maximum mesh size. We assume the mesh is regular, namely the ratio between the maximum and the minimum mesh sizes stays bounded during mesh refinements. We define the piecewise-polynomial space $V_h$ as the space of polynomials of the degree up to $k$ in each cell $I_j$, i.e.

$$V_h = \{v : \quad v \in P^k(I_j) \quad \text{for } x \in I_j, \quad j = 1, \ldots, N\}.$$

Note that functions in $V_h$ are allowed to have discontinuities across element interfaces.

The solution of the numerical scheme is denoted by $u_h$, which belongs to the finite element space $V_h$. We denote by $(u_h)_{j+\frac{1}{2}}^+$ and $(u_h)_{j+\frac{1}{2}}^-$ the values of $u_h$ at $x_{j+\frac{1}{2}}$, from the right cell $I_{j+1}$, and from the left cell $I_j$, respectively. We use the usual notations $[u_h] = u_h^+ - u_h^-$ and $\bar{u}_h = \frac{1}{2}(u_h^+ + u_h^-)$ to denote the jump and the mean of the function $u_h$ at each element boundary point, respectively.

## 2.2  The LDG method

In this section, we define our LDG method for the Camassa-Holm equation (1.1), written in the following form

$$u - u_{xx} = q, \tag{2.1}$$

$$q_t + f(u)_x = \frac{1}{2}(u^2)_{xxx} - \frac{1}{2}((u_x)^2)_x \tag{2.2}$$

with an initial condition

$$u(x, 0) = u_0(x) \tag{2.3}$$

and periodic boundary conditions

$$u(x, t) = u(x + L, t), \tag{2.4}$$

where $L$ is the period in the $x$ direction and $f(u) = 2\kappa u + \frac{3}{2}u^2$. Notice that the assumption of periodic boundary conditions is for simplicity only and is not essential: the method can be easily designed for non-periodic boundary conditions.

To define the local discontinuous Galerkin method, we further rewrite the equation (2.1) as a first order system:

$$u - r_x = q, \tag{2.5}$$
$$r - u_x = 0.$$

The LDG method for the equations (2.5), where $q$ is assumed known and we would want to solve for $u$, is formulated as follows: find $u_h$, $r_h \in V_h$ such that, for all test functions $\rho$, $\phi \in V_h$,

$$\int_{I_j} u_h \rho \, dx + \int_{I_j} r_h \rho_x \, dx - (\widehat{r}_h \rho^-)_{j+\frac{1}{2}} + (\widehat{r}_h \rho^+)_{j-\frac{1}{2}} = \int_{I_j} q_h \rho \, dx, \tag{2.6}$$

$$\int_{I_j} r_h \phi \, dx + \int_{I_j} u_h \phi_x \, dx - (\widehat{u}_h \phi^-)_{j+\frac{1}{2}} + (\widehat{u}_h \phi^+)_{j-\frac{1}{2}} = 0. \tag{2.7}$$

The "hat" terms in (2.6)–(2.7) in the cell boundary terms from integration by parts are the so-called "numerical fluxes", which are single valued functions defined on the edges and should be designed based on different guiding principles for different PDEs to ensure stability. For the standard elliptic equation (2.5), we can take the simple choices such that

$$\widehat{r}_h = r_h^-, \quad \widehat{u}_h = u_h^+, \tag{2.8}$$

where we have omitted the half-integer indices $j + \frac{1}{2}$ as all quantities in (2.8) are computed at the same points (i.e. the interfaces between the cells). We remark that the choice for the fluxes (2.8) is not unique. We can for example also choose the following numerical flux

$$\widehat{r}_h = r_h^+, \quad \widehat{u}_h = u_h^-. \tag{2.9}$$

For the equation (2.2), we can also rewrite it into a first order system:

$$q_t + f(u)_x - p_x + B(r)_x = 0,$$
$$p - (b(r)u)_x = 0, \qquad (2.10)$$
$$r - u_x = 0,$$

where $B(r) = \frac{1}{2}r^2$ and $b(r) = B'(r) = r$. Now we can define a local discontinuous Galerkin method to equations (2.10), resulting in the following scheme: find $q_h$, $p_h$, $r_h \in V_h$ such that, for all test functions $\varphi$, $\psi$, $\eta \in V_h$,

$$\int_{I_j} (q_h)_t \varphi dx - \int_{I_j} (f(u_h) - p_h + B(r_h))\varphi_x dx$$
$$+ ((\widehat{f} - \widehat{p}_h + \widehat{B(r_h)})\varphi^-)_{j+\frac{1}{2}} - ((\widehat{f} - \widehat{p}_h + \widehat{B(r_h)})\varphi^+)_{j-\frac{1}{2}} = 0, \qquad (2.11)$$

$$\int_{I_j} p_h \psi dx + \int_{I_j} b(r_h)u_h \psi_x dx - (\widehat{b(r_h)}\widetilde{u}_h \psi^-)_{j+\frac{1}{2}} + (\widehat{b(r_h)}\widetilde{u}_h \psi^+)_{j-\frac{1}{2}} = 0, \qquad (2.12)$$

$$\int_{I_j} r_h \phi dx + \int_{I_j} u_h \eta_x dx - (\widehat{u}_h \eta^-)_{j+\frac{1}{2}} + (\widehat{u}_h \eta^+)_{j-\frac{1}{2}} = 0. \qquad (2.13)$$

The numerical fluxes in equations (2.11)–(2.13) are chosen as

$$\widehat{p}_h = p_h^-, \ \widehat{u}_h = u_h^+, \ \widehat{B(r_h)} = B(r_h^-), \ \widehat{b(r_h)} = \frac{B(r_h^+) - B(r_h^-)}{r_h^+ - r_h^-}, \ \widetilde{u}_h = u_h^+. \qquad (2.14)$$

Here $\widehat{f}(u_h^-, u_h^+)$ is a monotone flux for solving conservation laws, i.e. it is Lipschitz continuous in both arguments, consistent ($\widehat{f}(u_h, u_h) = f(u_h)$), non-decreasing in the first argument and non-increasing in the second argument. Examples of monotone fluxes which are suitable for discontinuous Galerkin methods can be found in, e.g., [8]. We could for example use the simple Lax-Friedrichs flux

$$\widehat{f}(u_h^-, u_h^+) = \frac{1}{2}(f(u_h^-) + f(u_h^+) - \alpha(u_h^+ - u_h^-)), \quad \alpha = \max |f'(u_h)|,$$

where the maximum is taken over a relevant range of $u_h$. This Lax-Friedrichs flux is used in the numerical experiments in next section. The definition of the algorithm is now complete.

We remark that the choice for the fluxes (2.14) is not unique. In fact the crucial part is taking $\widehat{p}_h$ and $\widehat{u}_h$ from opposite sides and $\widehat{B(r_h)}$ and $\widetilde{u}_h$ from opposite sides.

## 2.3 Algorithm flowchart

In this section, we give details related to the implementation of the method.

- First, from the equations (2.6)-(2.8), we obtain $q_h$ in the following matrix form

$$\boldsymbol{q}_h = \mathbf{A}\boldsymbol{u}_h, \qquad (2.15)$$

where $\boldsymbol{q}_h$ and $\boldsymbol{u}_h$ are the vectors containing the degrees of freedom for $q_h$ and $u_h$, respectively.

- From (2.11)-(2.14), we obtain the LDG discretization of the residual $-f(u)_x + \frac{1}{2}(u^2)_{xxx} - \frac{1}{2}((u_x)^2)_x$ in the following vector form

$$(\boldsymbol{q}_h)_t = \mathbf{res}(\boldsymbol{u}_h). \tag{2.16}$$

- We then combine (2.15) and (2.16) to obtain

$$\mathbf{A}(\boldsymbol{u}_h)_t = \mathbf{res}(\boldsymbol{u}_h). \tag{2.17}$$

- We use a time discretization method to solve

$$(\boldsymbol{u}_h)_t = \mathbf{A}^{-1}\mathbf{res}(\boldsymbol{u}_h). \tag{2.18}$$

This step involves a linear solver with the matrix $\mathbf{A}$. We perform a *LU* decomposition for $\mathbf{A}$ at the beginning and use it for all time steps. Any standard ODE solvers can be used here, for example the Runge-Kutta methods.

The LDG matrix $\mathbf{A}$ is a sparse block matrix, hence its multiplication with vectors and a linear solver involving it as the coefficient matrix can be implemented efficiently.

# 3 $L^2$ stability of the LDG method

In this section, we prove the $L^2$ stability of the LDG method for the Camassa-Holm equation defined in the previous section.

**Proposition 3.1.** ($L^2$ stability) The solution to the schemes (2.6)-(2.8) and (2.11)-(2.14) satisfies the $L^2$ stability

$$\frac{d}{dt}\int_0^L (u_h^2 + r_h^2)dx \leq 0. \tag{3.1}$$

*Proof.* For equation (2.6), we first take the time derivative and get

$$\int_{I_j}(u_h)_t\rho dx + \int_{I_j}(r_h)_t\rho_x dx - (\widehat{(r_h)}_t\rho^-)_{j+\frac{1}{2}} + (\widehat{(r_h)}_t\rho^+)_{j-\frac{1}{2}} = \int_{I_j}(q_h)_t\rho dx. \tag{3.2}$$

Since (3.2), (2.7) and (2.11)–(2.13) holds for any test functions in $V_h$, we can choose

$$\rho = -u_h, \quad \phi = (r_h)_t, \quad \varphi = u_h, \quad \psi = -r_h, \quad \eta = p_h.$$

With these choices of test functions and summing up the five equations in (3.2), (2.7) and (2.11)–(2.13), we obtain

$$\int_{I_j}((u_h)_t u_h + (r_h)_t r_h)dx - \int_{I_j}f(u_h)(u_h)_x dx + (\widehat{f(u_h)}u_h^-)_{j+\frac{1}{2}} - (\widehat{f(u_h)}u_h^+)_{j-\frac{1}{2}}$$

$$+ \int_{I_j}(p_h u_h)_x dx - (\widehat{p}_h u_h^- + \widehat{u}_h p_h^-)_{j+\frac{1}{2}} + (\widehat{p}_h u_h^+ + \widehat{u}_h p_h^+)_{j-\frac{1}{2}}$$

6

$$-\int_{I_j} (B(r_h)u_h)_x dx + (\widehat{B(r_h)}u_h^- + \widehat{b(r_h)}\widetilde{u}_h r_h^-)_{j+\frac{1}{2}} - (B(r_h)u_h^+ + \widehat{b(r_h)}\widetilde{u}_h r_h^+)_{j-\frac{1}{2}}$$

$$+\int_{I_j} ((r_h)_t u_h)_x dx - (\widehat{(r_h)}_t u_h^- + \widehat{u}_h (r_h^-)_t)_{j+\frac{1}{2}} + (\widehat{(r_h)}_t u_h^+ + \widehat{u}_h (r_h^+)_t)_{j-\frac{1}{2}} = 0.$$

Taking $F(u_h) = \int^{u_h} f(\tau)d\tau$, we have

$$\int_{I_j} ((u_h)_t u_h + (r_h)_t r_h)dx + \Psi_{j+\frac{1}{2}} - \Psi_{j-\frac{1}{2}} + \Theta_{j-\frac{1}{2}} = 0, \qquad (3.3)$$

where the numerical entropy fluxes are given by

$$\Psi_{j+\frac{1}{2}} = \Big(-F(u_h^-) + \widehat{f}u_h^- + p_h^- u_h^- - (\widehat{p}_h u_h^- + \widehat{u}_h p_h^-)$$

$$-B(r_h^-)u_h^- + \widehat{B(r_h)}u_h^- + \widehat{b(r_h)}r_h^- + (r_h^-)_t u_h^- - (\widehat{(r_h)}_t u_h^- + \widehat{u}_h (r_h^-)_t)\Big)_{j+\frac{1}{2}},$$

and the extra term $\Theta$ is given by

$$\Theta_{j-\frac{1}{2}} = \Big([F(u_h)] - \widehat{f}[u_h] - [p_h u_h] + \widehat{p}_h[u_h] + \widehat{u}_h[p_h]$$

$$+ [B(r_h)u_h] - \widehat{b(r_h)}\widetilde{u}_h[r_h] - \widehat{B(r_h)}[u_h] - [(r_h)_t u_h] + \widehat{(r_h)}_t[u_h] + \widehat{u}_h[(r_h)_t]\Big)_{j-\frac{1}{2}}.$$

With the definition (2.8) and (2.14) of the numerical fluxes and after some algebraic manipulation, we easily obtain

$$-[p_h u_h] + \widehat{p}_h[u_h] + \widehat{u}_h[p_h] = 0,$$

$$[B(r_h)u_h] - \widehat{b(r_h)}\widetilde{u}_h[r_h] - \widehat{B(r_h)}[u_h] = 0,$$

$$-[(r_h)_t u_h] + \widehat{(r_h)}_t[u_h] + \widehat{u}_h[(r_h)_t] = 0$$

and hence

$$\Theta_{j-\frac{1}{2}} = ([F(u_h)] - \widehat{f}[u_h])_{j-\frac{1}{2}} \geq 0,$$

where the last inequality follows from the monotonicity of the flux

$$[F(u_h)] - \widehat{f}[u_h] = \int_{u_h^-}^{u_h^+} (f(s) - \widehat{f}(u_h^-, u_h^+))ds \geq 0.$$

Summing up the cell entropy inequalities, we obtain the desired $L^2$ stability (3.1). $\qquad \square$

# 4    Error estimates of the LDG method

In this section, we present the procedure to obtain *a priori* error estimates of the LDG method for the Camassa-Holm equation.

## 4.1 Notations, definitions and auxiliary result

In this section we introduce notations and definitions to be used later in the paper and also present some auxiliary results. We first review an important quantity measuring the relationship between the numerical flux and physical flux introduced in [34, 31]. We then define some projections and present certain interpolation and inverse properties for the finite element spaces that will be used in the error analysis.

### 4.1.1 Notations for different constants

We will adopt the following convention for different constants. These constants may have a different value in each occurrence.

We will denote by $C$ a positive constant independent of $h$, which may depend on the solution of the problem considered in this paper. Especially, to emphasize the nonlinearity of the flux $f(u)$ (or other nonlinear fluxes), we will denote by $C_\star$ a positive constant depending on the maximum of $|f''|$ or/and $|f'''|$. we remark that $C_\star = 0$ for a linear flux $f = cu$ with a constant $c$. For problems considered in this section, the exact solution is assumed to be smooth with periodic or compactly supported boundary condition. Also, $0 \leq t \leq T$ for a fixed $T$. Therefore, the exact solution is always bounded. We follow the convention [34] to redefine the nonlinear functions $f(u)$, $B(u)$, etc. outside their ranges such that the derivatives of these nonlinear functions $f'(u)$, $f''(u)$, etc. become globally bounded functions.

### 4.1.2 A quantity related to the numerical flux

For notational convenience we would like to introduce the following numerical flux related to the discontinuous Galerkin spatial discretization. $\widehat{f}(\omega^-, \omega^+)$ is a given monotone numerical flux that depends on the two values of the function $\omega$ at the discontinuity point $x_{j+\frac{1}{2}}$, namely $\omega^\pm_{j+\frac{1}{2}} = \omega(x^\pm_{j+\frac{1}{2}})$. The numerical flux $\widehat{f}(\omega^-, \omega^+)$ satisfies the following conditions:

(a) it is locally Lipschitz continuous, so it is bounded when $\omega^\pm$ are in a bounded interval;

(b) it is consistent with the flux $f(\omega)$, i.e., $\widehat{f}(\omega, \omega) = f(\omega)$;

(c) it is a nondecreasing function of its first argument, and a nonincreasing function of its second argument.

In [34], Zhang and Shu introduced an important quantity to measure the difference between the numerical flux and the physical flux. In [31], Xu and Shu introduced the idea of "uniform dissipative flux". For completeness, we give their definition in the following lemma.

**Lemma 4.1.** [34] *For any piecewise smooth function $\omega \in L^2(0,1)$, on each cell boundary point we define*

$$\alpha(\widehat{f}; \omega) \equiv \alpha(\widehat{f}; \omega^-, \omega^+) \triangleq \begin{cases} [\omega]^{-1}(f(\bar{\omega}) - \widehat{f}(\omega)), & \text{if} [\omega] \neq 0; \\ \frac{1}{2}|f'(\bar{\omega})|, & \text{if} [\omega] = 0, \end{cases} \tag{4.1}$$

*where $\widehat{f}(\omega) \equiv \widehat{f}(\omega^-, \omega^+)$ is a monotone numerical flux consistent with the given flux $f$. Then $\alpha(\widehat{f}; \omega)$ is non-negative and bounded for any $(\omega^-, \omega^+) \in \mathbb{R}^2$. Moreover we have*

$$\frac{1}{2}|f'(\bar{\omega})| \leq \alpha(\widehat{f}; \omega) + C_\star|[\omega]|, \tag{4.2}$$

$$-\frac{1}{8}f''(\bar{\omega})[\omega] \leq \alpha(\widehat{f}; \omega) + C_\star|[\omega]|^2. \tag{4.3}$$

**Remark 4.1.** Examples of monotone fluxes which are suitable for the discontinuous Galerkin methods can be found in, e.g., [8]. For our error estimates, we rewrite the numerical flux in a viscosity form

$$\widehat{f}(\omega^-, \omega^+) = \frac{1}{2}(f(\omega^-) + f(\omega^+) - \lambda(\omega^-, \omega^+)(\omega^+ - \omega^-)), \tag{4.4}$$

and assume the viscosity coefficient $\lambda(\omega^-, \omega^+)$ satisfies

$$\lambda(\omega^-, \omega^+) \geq \lambda_0 > 0, \quad \lambda_0 \text{ is constant.} \tag{4.5}$$

We call such flux as a "uniform dissipative flux" [31]. The well known Lax-Friedrichs flux is a uniform dissipative flux with a proper choice of $\lambda$. This property is necessary in our proof because of a lack of control for certain jump terms at cell boundaries due to the nonlinear terms and the high order derivative terms.

We would also like to use the following simplified notation. For any functions $\omega$ and $\phi$, we denote

$$\alpha(\widehat{f}; \omega)[\phi]^2 = \sum_{1 \leq j \leq N} \alpha(\widehat{f}; \omega)_{j+\frac{1}{2}}[\phi]^2_{j+\frac{1}{2}}.$$

### 4.1.3 Projection and interpolation properties

In what follows, we will consider the standard $L^2$-projection of a function $\omega$ with $k+1$ continuous derivatives into space $V_h$, denoted by $\mathcal{P}$, i.e., for each $j$,

$$\int_{I_j} (\mathcal{P}\omega(x) - \omega(x))v(x)dx = 0 \quad \forall v \in P^k(I_j), \tag{4.6}$$

and the special projection $\mathcal{P}^\pm$ into $V_h$, which satisfy, for each $j$,

$$\int_{I_j} (\mathcal{P}^+\omega(x) - \omega(x))v(x)dx = 0 \quad \forall v \in P^{k-1}(I_j), \quad \text{and} \quad \mathcal{P}^+\omega(x^+_{j-\frac{1}{2}}) = \omega(x_{j-\frac{1}{2}}) \tag{4.7}$$

$$\int_{I_j} (\mathcal{P}^-\omega(x) - \omega(x))v(x)dx = 0 \quad \forall v \in P^{k-1}(I_j), \quad \text{and} \quad \mathcal{P}^-\omega(x^-_{j+\frac{1}{2}}) = \omega(x_{j+\frac{1}{2}}).$$

For the projections mentioned above, it is easy to show (c.f. [6])

$$\|\omega^e\| + h\|\omega^e\|_\infty + h^{\frac{1}{2}}\|\omega^e\|_{\Gamma_h} \le Ch^{k+1}, \tag{4.8}$$

where $\omega^e = \mathcal{P}\omega - \omega$ or $\omega^e = \mathcal{P}^{\pm}\omega - \omega$. The positive constant $C$, solely depending on $\omega$, is independent of $h$. $\Gamma_h$ denotes the set of boundary points of all elements $I_j$.

### 4.1.4 Inverse Properties

Finally we list some inverse properties of the finite element space $V_h$ that will be used in our error analysis. For any $\omega_h \in V_h$, there exists a positive constant $C$ independent of $\omega_h$ and $h$, such that

(i) $\|\partial_x \omega_h\| \le Ch^{-1}\|\omega_h\|,$   (ii) $\|\omega_h\|_{\Gamma_h} \le Ch^{-\frac{1}{2}}\|\omega_h\|,$   (iii) $\|\omega_h\|_\infty \le Ch^{-\frac{1}{2}}\|\omega_h\|.$   (4.9)

For more details of these inverse properties, we refer to [6].

## 4.2 The main error estimate result

We state the main error estimates of the semi-discrete LDG scheme for the Camassa-Holm equation.

**Theorem 4.2.** *Let $u$ be the exact solution of the problem (2.1)-(2.2), which is sufficiently smooth with bounded derivatives, and assume $f \in C^3$. Let $u_h$ be the numerical solution of the semi-discrete LDG scheme (2.6)-(2.8) and (2.11)-(2.14) and denote the corresponding numerical error by $e_u = u - u_h$ and $e_r = r - r_h$ where $r = u_x$ is defined by (2.5). For regular triangulations of $I = (0,1)$, if the finite element space $V_h$ is the piecewise polynomials of degree $k \ge 2$, then for small enough $h$ there holds the following error estimates*

$$\|u - u_h\|^2 + \|r - r_h\|^2 \le Ch^{2k}, \tag{4.10}$$

*where the constant $C$ depends on the final time $T$, $k$, $\|u\|_{k+1}$, $\|r\|_{k+1}$ and the bounds on the derivatives $|f^{(m)}|$, $m = 1, 2, 3$. Here $\|u\|_{k+1}$ and $\|r\|_{k+1}$ are the maximum over $0 \le t \le T$ of the standard Sobolev $k + 1$ norm in space.*

**Remark 4.2.** Although we could not obtain the optimal error estimates $O(h^{k+1})$ for $u$ due to some extra boundary terms arising from high order derivatives, numerical examples in Section 5 verify the optimal order $O(h^{k+1})$ for $u$. For the solution $r_h$, our numerical results indicate that $k$-th order accuracy is sharp.

### 4.2.1 The error equation

In order to obtain the error estimate to smooth solutions for the considered semi-discrete LDG scheme (2.6)-(2.8) and (2.11)-(2.14), we need to first obtain the error equation.

Notice that the scheme (2.6) and (2.11)–(2.13) is also satisfied when the numerical solutions are replaced by the exact solutions. We then obtain the error equation

$$\int_{I_j} (u - u_h)_t \rho\, dx - \int_{I_j} \Big( (q - q_h)_t(\rho + \varphi) + (r - r_h)\phi + (p - p_h)\psi + (r - r_h)\eta \Big) dx$$

$$+ \int_{I_j} (r - r_h)_t \rho_x\, dx - ((r_t - \widehat{(r_h)}_t)\rho^-)_{j+\frac{1}{2}} + ((r_t - \widehat{(r_h)}_t)\rho^+)_{j-\frac{1}{2}}$$

$$+ \int_{I_j} (u - u_h)\phi_x\, dx - ((u - \widehat{u}_h)\phi^-)_{j+\frac{1}{2}} + ((u - \widehat{u}_h)\phi^+)_{j-\frac{1}{2}}$$

$$+ \int_{I_j} (p - p_h)\varphi_x\, dx - ((p - \widehat{p}_h)\varphi^-)_{j+\frac{1}{2}} + ((p - \widehat{p}_h)\varphi^+)_{j-\frac{1}{2}}$$

$$+ \int_{I_j} (u - u_h)\eta_x\, dx - ((u - \widehat{u}_h)\eta^-)_{j+\frac{1}{2}} + ((u - \widehat{u}_h)\eta^+)_{j-\frac{1}{2}}$$

$$- \int_{I_j} (B(r) - B(r_h))\varphi_x\, dx + ((B(r) - \widehat{B(r_h)})\varphi^-)_{j+\frac{1}{2}} - ((B(r) - \widehat{B(r_h)})\varphi^+)_{j-\frac{1}{2}}$$

$$+ \int_{I_j} (b(r)u - b(r_h)u_h)\psi_x\, dx - ((b(r)u - \widehat{b(r_h)\widetilde{u}_h})\psi^-)_{j+\frac{1}{2}} + ((b(r)u - \widehat{b(r_h)\widetilde{u}_h})\psi^+)_{j-\frac{1}{2}}$$

$$- \int_{I_j} (f(u) - f(u_h))\varphi_x\, dx + ((f(u) - \widehat{f})\varphi^-)_{j+\frac{1}{2}} - ((f(u) - \widehat{f})\varphi^+)_{j-\frac{1}{2}} = 0$$

for all $\rho, \phi, \varphi, \psi, \eta \in V_h$.

Define

$$\mathcal{B}_j(u - u_h, q - q_h, p - p_h, r - r_h; \rho, \phi, \varphi, \psi, \eta)$$

$$= \int_{I_j} (u - u_h)_t \rho\, dx - \int_{I_j} \Big( (q - q_h)_t(\rho + \varphi) + (r - r_h)\phi + (p - p_h)\psi + (r - r_h)\eta \Big) dx$$

$$+ \int_{I_j} (r - r_h)_t \rho_x\, dx - ((r_t - \widehat{(r_h)}_t)\rho^-)_{j+\frac{1}{2}} + ((r_t - \widehat{(r_h)}_t)\rho^+)_{j-\frac{1}{2}}$$

$$+ \int_{I_j} (u - u_h)\phi_x\, dx - ((u - \widehat{u}_h)\phi^-)_{j+\frac{1}{2}} + ((u - \widehat{u}_h)\phi^+)_{j-\frac{1}{2}} \qquad (4.11)$$

$$+ \int_{I_j} (p - p_h)\varphi_x\, dx - ((p - \widehat{p}_h)\varphi^-)_{j+\frac{1}{2}} + ((p - \widehat{p}_h)\varphi^+)_{j-\frac{1}{2}}$$

$$+ \int_{I_j} (u - u_h)\eta_x\, dx - ((u - \widehat{u}_h)\eta^-)_{j+\frac{1}{2}} + ((u - \widehat{u}_h)\eta^+)_{j-\frac{1}{2}},$$

$$\mathcal{H}_j(f; u, u_h; \varphi) = \int_{I_j} (f(u) - f(u_h))\varphi_x\, dx - ((f(u) - \widehat{f})\varphi^-)_{j+\frac{1}{2}} + ((f(u) - \widehat{f})\varphi^+)_{j-\frac{1}{2}},$$

$$(4.12)$$

and

$$\mathbf{R}_j(b, B; r, u, r_h, u_h; \varphi, \psi) \qquad (4.13)$$

$$= \int_{I_j} (B(r) - \widehat{B(r_h)})\varphi_x dx - ((B(r) - \widehat{B(r_h)})\varphi^-)_{j+\frac{1}{2}} + ((B(r) - \widehat{B(r_h)})\varphi^+)_{j-\frac{1}{2}}$$

$$- \int_{I_j} (b(r)u - b(r_h)u_h)\psi_x dx + ((b(r)u - \widehat{b(r_h)}\widetilde{u}_h)\psi^-)_{j+\frac{1}{2}} - ((b(r)u - \widehat{b(r_h)}\widetilde{u}_h)\psi^+)_{j-\frac{1}{2}}.$$

Summing over $j$, the error equation becomes

$$\sum_{j=1}^{N} \mathcal{B}_j(u - u_h, q - q_h, p - p_h, r - r_h; \rho, \phi, \varphi, \psi, \eta) \tag{4.14}$$

$$= \sum_{j=1}^{N} \Big( \mathcal{H}_j(f; u, u_h; \varphi) + \mathbf{R}_j(b, B; r, u, r_h, u_h; \varphi, \psi) \Big)$$

for all $\rho$, $\phi$, $\varphi$, $\psi$, $\eta \in V_h$.

Denoting

$$\begin{aligned}
s &= \mathcal{P}^+ u - u_h, & s^e &= \mathcal{P}^+ u - u, \\
\xi &= \mathcal{P}q - q_h, & \xi^e &= \mathcal{P}q - q, \\
v &= \mathcal{P}p - p_h, & v^e &= \mathcal{P}p - p, \\
\sigma &= \mathcal{P}r - r_h, & \sigma^e &= \mathcal{P}r - r
\end{aligned} \tag{4.15}$$

and taking the test functions

$$\rho = -s, \quad \phi = \sigma_t, \quad \varphi = s, \quad \psi = -\sigma, \quad \eta = v,$$

we obtain the important *energy equality*

$$\sum_{j=1}^{N} \mathcal{B}_j(s - s^e, \xi - \xi^e, v - v^e, \sigma - \sigma^e; -s, \sigma_t, s, -\sigma, v) \tag{4.16}$$

$$= \sum_{j=1}^{N} \Big( \mathcal{H}_j(f; u, u_h; s) + \mathbf{R}_j(b, B; r, u, r_h, u_h; s, -\sigma) \Big).$$

### 4.2.2 Proof of the main result

In this subsection, we will follow the idea of [31] to present the main proof of Theorem 4.2. We shall prove the theorem by analyzing each term of the energy equation (4.16).

First, we consider the left hand side of the energy equation (4.16). The estimates for the left hand side of the energy equation are given in the lemma below. The proof of this lemma will be given in the Appendix A.1.

**Lemma 4.3.** *The following equation holds*

$$\sum_{j=1}^{N} \mathcal{B}_j(s - s^e, \xi - \xi^e, v - v^e, \sigma - \sigma^e; -s, \sigma_t, s, -\sigma, v) \tag{4.17}$$

$$= \int_0^1 (ss_t + \sigma_t \sigma) dx - \int_0^1 s_t^e s \, dx - \sum_{j=1}^{N} ((\widehat{v^e} + \widehat{\sigma_t^e})[s])_{j+\frac{1}{2}}.$$

To deal with the nonlinearity of the flux $f(u)$ we would like to make an *a priori* assumption that, for small enough $h$, there holds

$$\|u - u_h\| \le h. \tag{4.18}$$

We will justify the validity of this *a priori* assumption later. For the linear flux $f(u) = cu$, this *a priori* assumption is unnecessary.

**Corollary 4.4.** Suppose that the interpolation property (4.8) is satisfied, then the a priori assumption (4.18) implies that

$$\|e_u\|_\infty \le Ch^{\frac{1}{2}} \quad and \quad \|\mathbb{Q}u - u_h\|_\infty \le Ch^{\frac{1}{2}} \tag{4.19}$$

where $\mathbb{Q} = \mathcal{P}$ or $\mathbb{Q} = \mathcal{P}^{\pm}$ is the projection operator.

Next, we consider the right hand side of the energy equation (4.16). We can rewrite it into the following form

$$\sum_{j=1}^{N} \mathcal{H}_j(f; u, u_h; s) = \sum_{j=1}^{N} \int_{I_j} (f(u) - f(u_h)) s_x dx \tag{4.20}$$

$$+ \sum_{j=1}^{N} ((f(u) - f(\bar{u}_h))[s])_{j+\frac{1}{2}} + \sum_{j=1}^{N} ((f(\bar{u}_h) - \widehat{f})[s])_{j+\frac{1}{2}},$$

$$\sum_{j=1}^{N} \mathbf{R}_j(b, B; r, u, r_h, u_h; s, -\sigma)$$

$$= \sum_{j=1}^{N} \int_{I_j} (B(r) - B(r_h)) s_x dx + \sum_{j=1}^{N} ((B(r) - B(r_h^-))[s])_{j+\frac{1}{2}} \tag{4.21}$$

$$+ \sum_{j=1}^{N} \int_{I_j} (b(r)u - b(r_h)u_h) \sigma_x dx + \sum_{j=1}^{N} ((b(r)u - \widehat{b}(r_h)u_h^+)[\sigma])_{j+\frac{1}{2}},$$

where we take into account the periodic boundary condition and recall the average $\bar{u}_h$ is defined by $\bar{u}_h = \frac{1}{2}(u_h^+ + u_h^-)$.

The estimates for the equation (4.20) are given in the lemma below.

**Lemma 4.5.** *Suppose that the interpolation properties (4.8) are satisfied, then we have the following estimate for (4.20)*

$$\sum_{j=1}^{N} \mathcal{H}_j(f; u, u_h; s) \tag{4.22}$$

$$\le -\frac{1}{4}\alpha(\widehat{f}; u_h)[s]^2 + (C + C_\star(\|s\|_\infty + h^{-1}\|e_u\|_\infty^2))\|s\|^2 + (C + C_\star h^{-1}\|e_u\|_\infty^2)h^{2k+1}.$$

**Remark 4.3.** For the proof of this lemma, we refer readers to Lemma 3.4 and Lemma 3.5 in [31]. For $f(u) = 2\kappa u + \frac{3}{2}u^2$ in the CH equation (1.1), we have $f'''(u) = 0$ and we do not need the estimate for $\mathcal{T}_6$ in [31].

The estimates for the equation (4.21) are given in the lemma below. The proof of this lemma will be given in the Appendix A.2.

**Lemma 4.6.** *Suppose that the interpolation properties (4.8) are satisfied, then we have the following estimate for (4.21)*

$$|\sum_{j=1}^{N}\mathbf{R}_j(b,B;r,u,r_h,u_h;s,-\sigma)| \tag{4.23}$$

$$\leq \sum_{j=1}^{N}(|b'(r)u\bar{\sigma}^e[\sigma]| + |b(r)(\sigma^e)^-[s]|)_{j+\frac{1}{2}} + \frac{1}{2}\|s\|^2 + C\|\sigma\|^2 + Ch^{2k+2}.$$

Now we are ready to get the final error estimates (4.10). Combining equations (4.16), (4.17), (4.22) and (4.23), we obtain

$$\int_0^1 (s_t s + \sigma_t \sigma)dx + \frac{1}{4}\alpha(\widehat{f};u_h)[s]^2$$

$$\leq \int_0^1 s_t^e s\,dx + \sum_{j=1}^{N}((\widehat{v^e} + \widehat{\sigma_t^e})[s])_{j+\frac{1}{2}} + \sum_{j=1}^{N}(|b'(r)u\bar{\sigma}^e[\sigma]| + |b(r)(\sigma^e)^-[s]|)_{j+\frac{1}{2}}$$

$$+ (C + C_\star(\|s\|_\infty + h^{-1}\|e_u\|_\infty^2))\|s\|^2 + (C + C_\star h^{-1}\|e_u\|_\infty^2)h^{2k+1} + C\|\sigma\|^2.$$

Again by Young's inequality and the interpolation property (4.8), the equation becomes

$$\int_0^1 (s_t s + \sigma_t \sigma)dx + \frac{1}{8}\alpha(\widehat{f};u_h)[s]^2$$

$$\leq (C + C_\star(\|s\|_\infty + h^{-1}\|e_u\|_\infty^2))\|s\|^2 + (C + C_\star h^{-1}\|e_u\|_\infty^2)h^{2k+1} + Ch^{2k} + C\|\sigma\|^2.$$

where we use the uniform dissipation property of the numerical flux $\widehat{f}$. Using the results (4.19) implied by the *a priori* assumption (4.18) and the positive property of $\alpha(\widehat{f};u_h)$, we can get the following error estimate

$$\frac{1}{2}\frac{d}{dt}\int_0^1 (s^2 + \sigma^2)dx \leq C(\|s\|^2 + \|\sigma\|^2) + Ch^{2k}.$$

Thus Theorem 4.2 follows by the triangle inequality and the interpolating property (4.8).

To complete the proof, let us verify the *a priori* assumption (4.18). For $k \geq 2$, we can consider $h$ small enough so that $Ch^k < \frac{1}{2}h$, where $C$ is the constant in (4.10) determined by the final time $T$. Then, if $t^* = \sup\{t : \|u(t) - u_h(t)\| \leq h\}$, we would have $\|u(t^*) - u_h(t^*)\| = h$ by continuity if $t^*$ is finite. On the other hand, our proof implies that (4.10) holds for $t \leq t^*$, in particular $\|u(t^*) - u_h(t^*)\| \leq Ch^k < \frac{1}{2}h$. This is a contradiction if $t^* < T$. Hence $t^* \geq T$ and our *a priori* assumption (4.18) is justified.

# 5    Numerical results

In this section we provide numerical examples to illustrate the accuracy and capability of the method. Time discretization is by the third order explicit TVD Runge-Kutta

14

method in [26]. This is not the most efficient method for the time discretization to our LDG scheme. However, we will not address the issue of time discretization efficiency in this paper. We have verified with the aid of successive mesh refinements, that in all cases, the results shown are numerically convergent. We will give the numerical test results for the CH equation

$$u_t - u_{xxt} + 3uu_x = 2u_x u_{xx} + uu_{xxx} \tag{5.1}$$

with different initial conditions.

## Example 5.1. Smooth solution

In this example, we test the scheme with smooth traveling waves. Smooth traveling waves are solution of the form

$$u(x,t) = \phi(x - ct) \tag{5.2}$$

where $\phi$ is solution of second-order ordinary differential equation

$$\phi_{xx} = \phi - \frac{\alpha}{(\phi - c)^2}. \tag{5.3}$$

In order to get a smooth traveling wave, we choose the constants $c$ and $\alpha$ as in [16], i.e. $\alpha = c = 3$. The initial conditions for $\phi$ is

$$\phi(0) = 1, \quad \frac{d\phi}{dx}(0) = 0. \tag{5.4}$$

It gives rise to a smooth traveling wave with period $a \simeq 6.46954603635$. We use fourth-order explicit Runge-Kutta method with 100000 points to approximate the solution of the equation (5.3). This high precision solution is used as a reference solution for the smooth traveling wave. The $L^2$ and $L^\infty$ errors and the numerical orders of accuracy for $u$ at time $t = 0.5$ with uniform meshes are contained in Table 5.1. Periodic boundary conditions are used. We can see that the method with $P^k$ elements gives a uniform $(k+1)$-th order of accuracy for $u$ in both norms. For the solution $r_h$, the accuracy is $k$-th order in both norms for $k \geq 1$ and this indicates that our error estimates result for $r$ is sharp.

## Example 5.2. Accuracy test

The peakon solutions of the CH equation (5.1) are well known and are the only traveling waves for which there is a simple explicit formula. The peaked traveling wave solution is

$$u(x,t) = ce^{-|x-ct|}, \tag{5.5}$$

where $c$ is the wave speed. We give the accuracy test with $c = 0.25$. The accuracy is measured in smooth parts of the solution, $1/5$ of the computational domain away from the peak. The $L^2$ and $L^\infty$ errors and the numerical orders of accuracy for $u$ at time $t = 1$ with uniform meshes in $[-25, 25]$ are contained in Table 5.2. We can see that the method with $P^k$ elements gives a uniform $(k+1)$-th order of accuracy for $u$ in both norms.

15

Table 5.1: Accuracy test for the CH equation (5.1) with the exact solution (5.2). Periodic boundary condition. Uniform meshes with $N$ cells at time $t = 0.5$.

| | $N$ | $u - u_h$ | | | | $r - r_h$ | | | |
|---|---|---|---|---|---|---|---|---|---|
| | | $L^2$ error | order | $L^\infty$ error | order | $L^2$ error | order | $L^\infty$ error | order |
| $P^0$ | 10 | 1.42E-01 | – | 3.08E-01 | – | 1.42E-01 | – | 3.08E-01 | – |
| | 20 | 7.95E-02 | 0.84 | 1.77E-01 | 0.80 | 7.95E-02 | 0.83 | 1.77E-01 | 0.57 |
| | 40 | 4.23E-02 | 0.91 | 9.41E-01 | 0.91 | 4.23E-02 | 0.94 | 9.41E-02 | 0.87 |
| | 80 | 2.18E-02 | 0.95 | 4.83E-02 | 0.96 | 2.18E-02 | 0.98 | 4.83E-02 | 0.97 |
| $P^1$ | 10 | 1.16E-02 | – | 6.63E-02 | – | 1.16E-02 | – | 6.63E-02 | – |
| | 20 | 3.12E-03 | 1.90 | 1.86E-02 | 1.84 | 3.12E-03 | 0.68 | 1.86E-02 | 0.24 |
| | 40 | 8.05E-04 | 1.95 | 4.76E-03 | 1.96 | 8.05E-04 | 0.85 | 4.76E-03 | 0.63 |
| | 80 | 2.04E-04 | 1.98 | 1.19E-02 | 2.00 | 2.04E-04 | 0.93 | 1.19E-03 | 0.87 |
| $P^2$ | 10 | 1.41E-03 | – | 6.75E-03 | – | 1.41E-03 | – | 6.75E-03 | – |
| | 20 | 1.49E-04 | 3.24 | 9.06E-04 | 2.90 | 1.49E-04 | 2.64 | 9.06E-04 | 2.64 |
| | 40 | 1.70E-05 | 3.13 | 9.85E-05 | 3.20 | 1.70E-05 | 2.06 | 9.85E-05 | 1.45 |
| | 50 | 8.95E-06 | 2.88 | 4.96E-05 | 3.07 | 8.95E-06 | 1.95 | 4.96E-05 | 1.77 |

Table 5.2: Accuracy test for the CH equation (5.1) with the exact solution (5.5). Periodic boundary condition. $c = 0.25$. Uniform meshes with $N$ cells at time $t = 1$.

| | $N$ | $L^2$ error | order | $L^\infty$ error | order |
|---|---|---|---|---|---|
| $P^0$ | 10 | 8.71E-03 | – | 1.90E-02 | – |
| | 20 | 2.18E-03 | 2.00 | 4.95E-03 | 1.94 |
| | 40 | 9.58E-04 | 1.18 | 2.36E-03 | 1.07 |
| | 80 | 4.08E-04 | 1.23 | 1.19E-03 | 0.98 |
| $P^1$ | 10 | 1.45E-02 | – | 3.17E-02 | – |
| | 20 | 8.33E-04 | 4.12 | 2.06E-03 | 3.94 |
| | 40 | 1.14E-04 | 2.87 | 3.74E-04 | 2.46 |
| | 80 | 1.80E-05 | 2.67 | 8.82E-05 | 2.08 |
| $P^2$ | 10 | 1.60E-02 | – | 3.50E-02 | – |
| | 20 | 4.05E-04 | 5.31 | 1.23E-03 | 4.83 |
| | 40 | 2.81E-05 | 3.85 | 9.65E-05 | 3.68 |
| | 80 | 3.54E-06 | 2.99 | 1.29E-05 | 2.90 |

## Example 5.3. Peakon solution

In this example, we present the wave propagation of the periodized version of the

solution (5.5). In the single peak case, the initial condition is

$$u_0(x) = \begin{cases} \dfrac{c}{\cosh(a/2)} \cosh(x - x_0), & |x - x_0| \le a/2, \\[3mm] \dfrac{c}{\cosh(a/2)} \cosh(a - (x - x_0)), & |x - x_0| > a/2, \end{cases} \tag{5.6}$$

where $x_0$ is the position of the trough and $a$ is the period. We present the wave propagation for the CH equation with parameters $c = 1$, $a = 30$ and $x_0 = -5$. The computational domain is $[0, a]$. In Figure 5.1, the peak profile at $t = 0$, 5, 10 and the space time graph of the solutions up to $t = 10$ are shown. The lack of smoothness at the peak of peakon introduces high-frequency dispersive errors into the calculation and will cause the numerical oscillation near the peak. In our computation of the LDG method, we use the $P^5$ element with $N = 320$ cells to resolve the peak. We can see clearly that the moving peak profile is resolved very well.

## Example 5.4. Two-peakon interaction

In this example we consider the two-Peakon interaction of the CH equation with the initial condition

$$u_0(x) = \phi_1(x) + \phi_2(x), \tag{5.7}$$

where

$$\phi_i(x) = \begin{cases} \dfrac{c_i}{\cosh(a/2)} \cosh(x - x_i), & |x - x_i| \le a/2, \\[3mm] \dfrac{c_i}{\cosh(a/2)} \cosh(a - (x - x_i)), & |x - x_i| > a/2, \end{cases} \qquad i = 1, 2. \tag{5.8}$$

The parameters are $c_1 = 2$, $c_2 = 1$, $x_1 = -5$, $x_2 = 5$, $a = 30$. The computational domain is $[0, a]$. We use the $P^5$ element with $N = 320$ cells in our computation of the LDG method. In Figure 5.2, the two-peakon interaction at $t = 0$, 5, 12 and 18 are shown. We can see clearly that the moving peak interaction is resolved very well.

## Example 5.5. Three-peakon interaction

In this example we consider the three-Peakon interaction of the CH equation with the initial condition

$$u_0(x) = \phi_1(x) + \phi_2(x) + \phi_3(x), \tag{5.9}$$

where $\phi_i$, $i = 1, 2, 3$ are defined as in (5.8). The parameters are $c_1 = 2$, $c_2 = 1$, $c_3 = 0.8$, $x_1 = -5$, $x_2 = -3$, $x_3 = -1$, $a = 30$. The computational domain is $[0, a]$. We use the $P^5$ element with $N = 320$ cells in our computation of the LDG method. In Figure 5.3, the three-peakon interaction at $t = 0$, 1, 2, 3, 4 and 6 are shown. We can see clearly that the moving peak interaction is resolved very well.
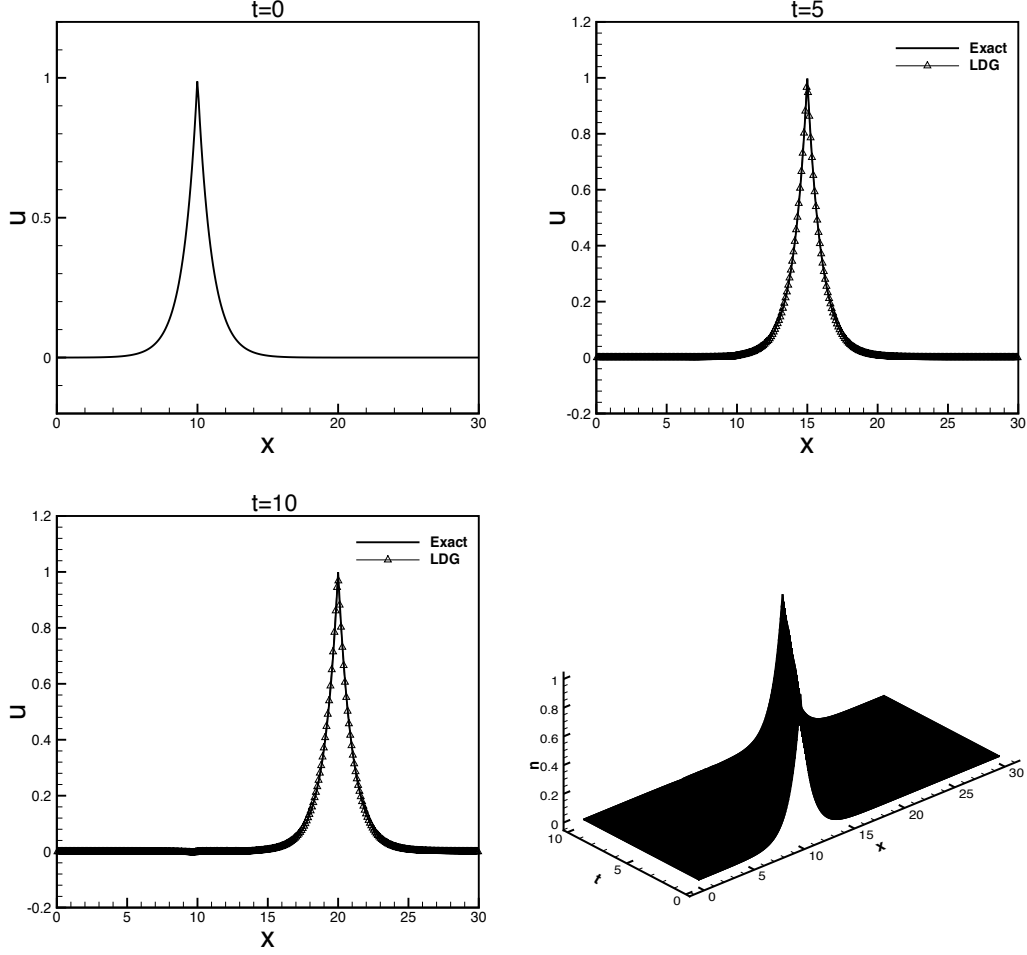
Figure 5.1: The peak profile of the CH equation (5.1) with the initial condition (5.6). Periodic boundary condition in $[0, 30]$. $P^5$ elements and a uniform mesh with $N = 320$ cells.

### Example 5.6. Solution with a discontinuous derivative

In this example we consider a initial data function $u_0$ which has a discontinuous derivative as in [16]. The initial condition is

$$u_0(x) = \frac{10}{(3 + |x|)^2}. \tag{5.10}$$

The computational domain is $[-30, 30]$. We use the $P^2$ element with $N = 640$ cells in our computation of the LDG method. The solutions at time $t = 5$, 10, 15 and 20 are shown in Figure 5.4. Even if we do not use higher order polynomials and more cells, we still obtain a good resolution of the solution comparable with that in [16].

### Example 5.7. Break up of the plateau traveling wave

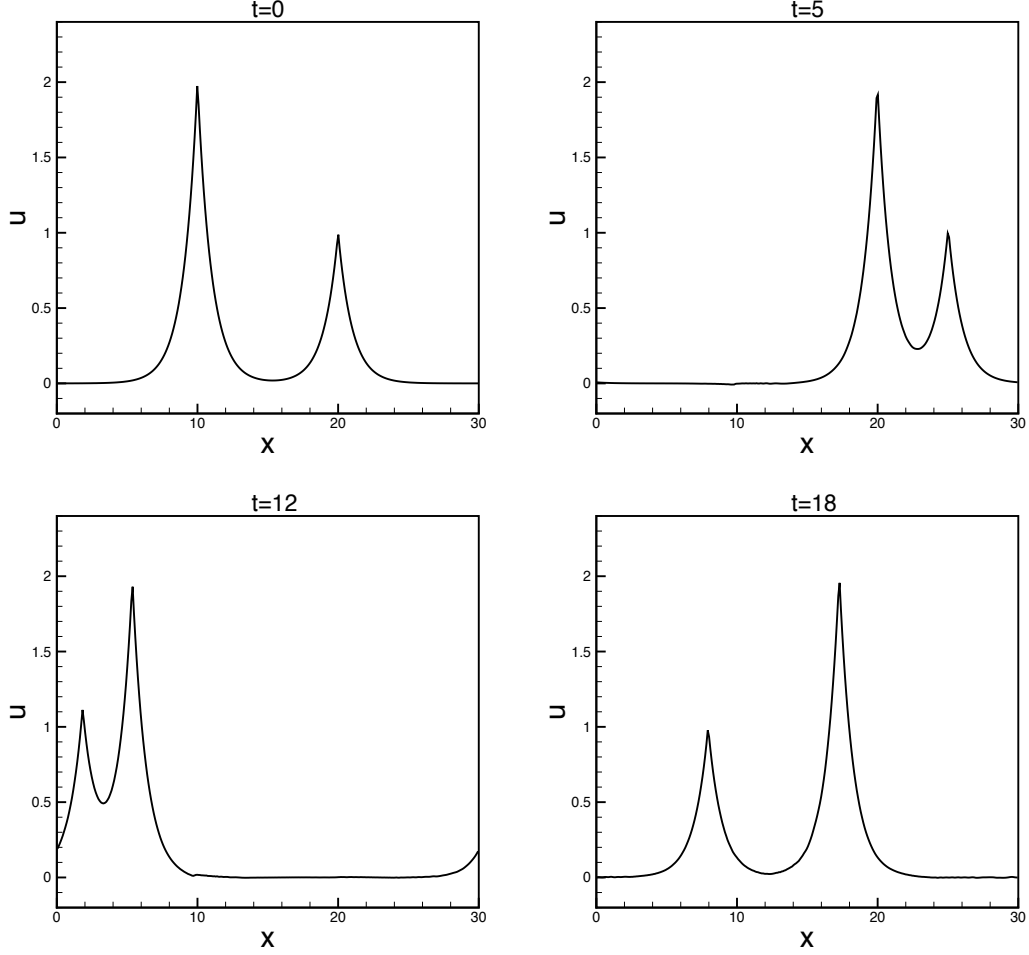In this example we consider a cut-off peakon in [1], i.e. a plateau function $u(x, t) =$

18

Figure 5.2: The two-peakon interaction of the CH equation (5.1) with the initial condition (5.7). Periodic boundary condition in $[0, 30]$. $P^5$ elements and a uniform mesh with $N = 320$ cells.

$\phi(x - ct)$ with

$$
\phi(x) = \begin{cases} ce^{x+k}, & x \leq -k, \\ c, & |x| \leq k, \\ ce^{-x+k}, & x \geq k. \end{cases} \tag{5.11}
$$

We put $c = 0.6$ and $k = 5$. The computational domain is $[-40, 40]$. We use the $P^2$ element with $N = 800$ cells in our computation of the LDG method. The break up of the plateau traveling wave is shown in Figure 5.5 at different time. The solution is resolved very well comparing with the result in [1].

# 6    Conclusion

We have developed a local discontinuous Galerkin method to solve the Camassa-Holm equation. $L^2$ stability is proven for general solutions, and an *a priori* error estimate
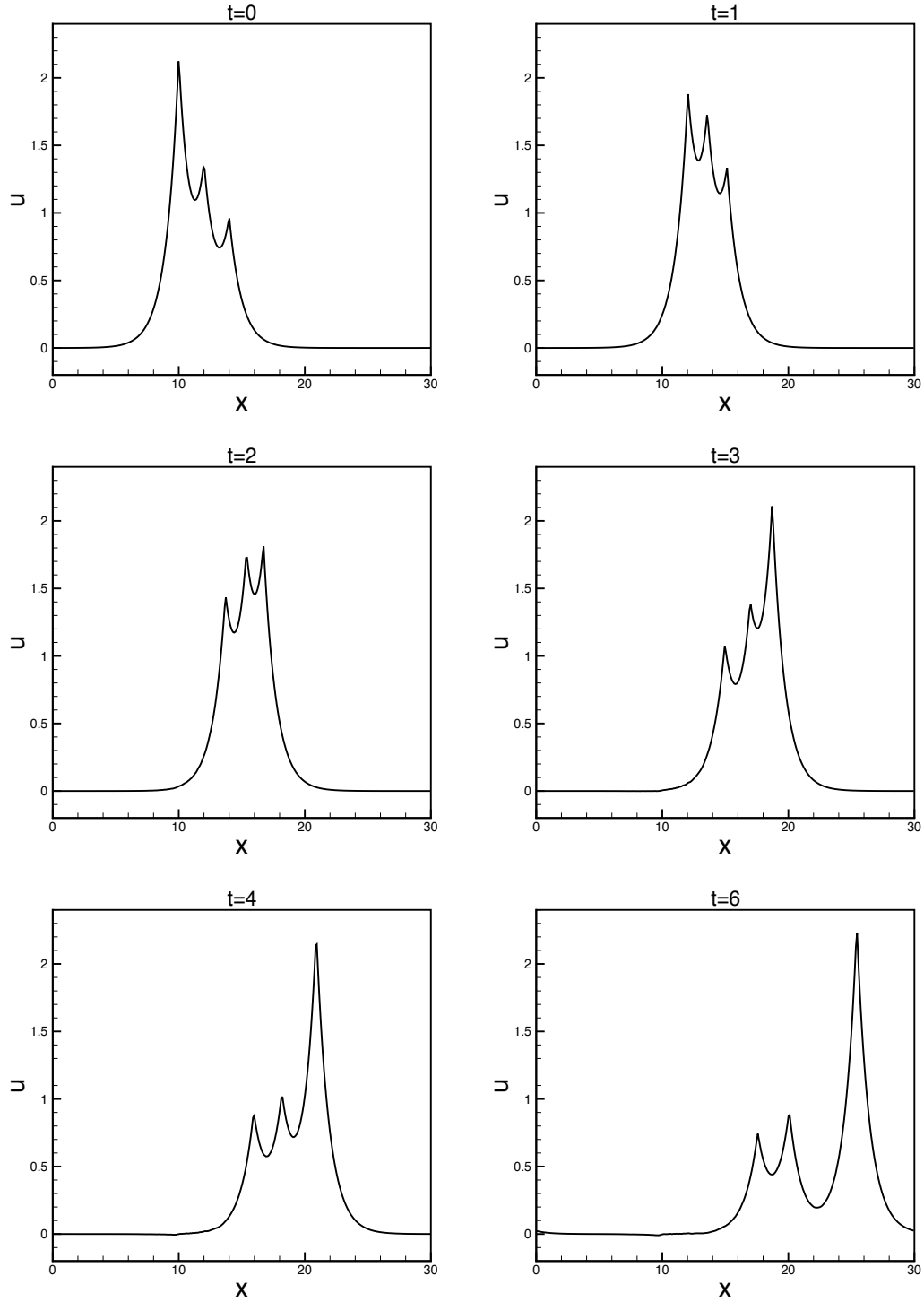
Figure 5.3: The three-peakon interaction of the CH equation (5.1) with the initial condition (5.9). Periodic boundary condition in $[0, 30]$. $P^5$ elements and a uniform mesh with $N = 320$ cells.
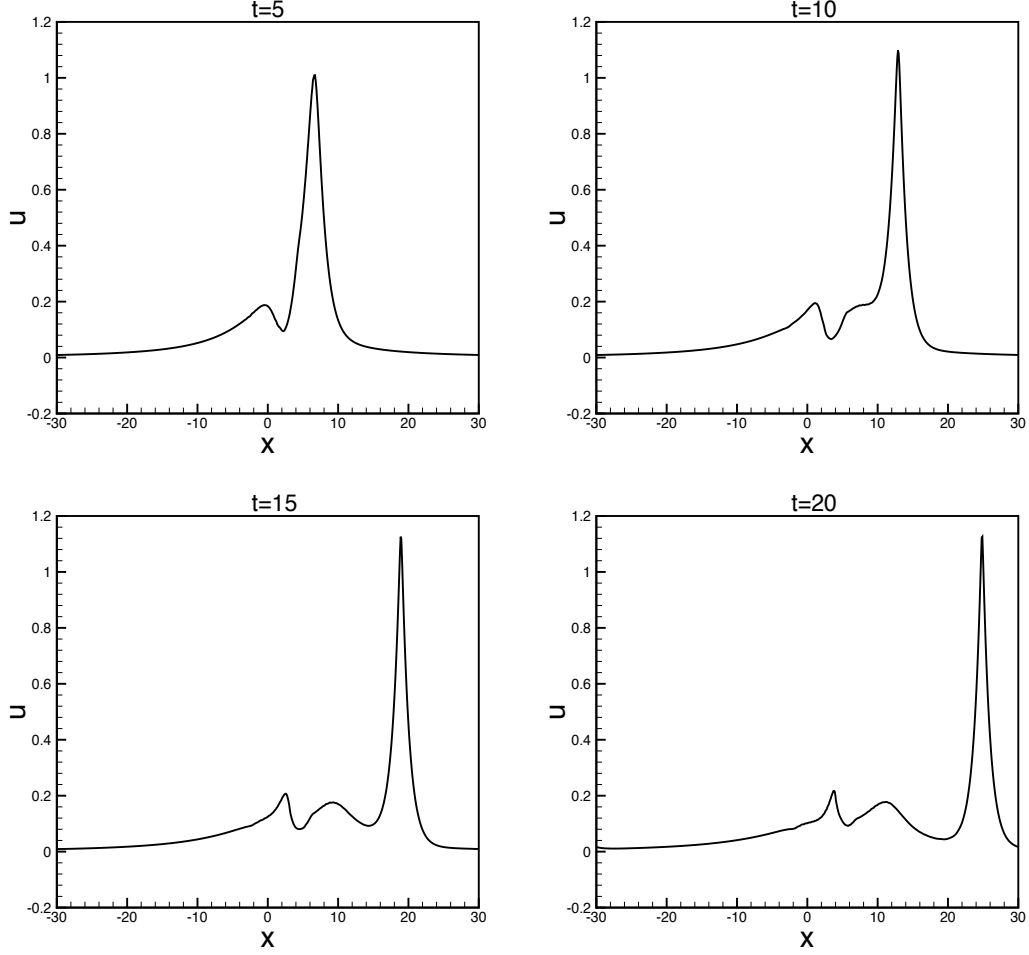
Figure 5.4: The solution with discontinuous derivative of the CH equation (5.1) with the initial condition (5.10). Periodic boundary condition in $[-30, 30]$. $P^2$ elements and a uniform mesh with $N = 640$ cells.

is obtained for smooth solutions. Numerical examples are given to illustrate the accuracy and capability of the methods. Although not addressed in this paper, the LDG methods are flexible for general geometry, unstructured meshes and $h$-$p$ adaptivity, and have excellent parallel efficiency. The LDG method has a good potential in solving the Camassa-Holm equation and similar nonlinear equations in mathematical physics.

# A    Appendix: Proof of several Lemmas

## A.1    Proof of Lemma 4.3

$$\mathcal{B}_j(s - s^e, \xi - \xi^e, v - v^e, \sigma - \sigma^e; -s, \sigma_t, s, -\sigma, v) \tag{A.1}$$
$$= \mathcal{B}_j(s, \xi, v, \sigma; -s, \sigma_t, s, -\sigma, v) - \mathcal{B}_j(s^e, \xi^e, v^e, \sigma^e; -s, \sigma_t, s, -\sigma, v),$$
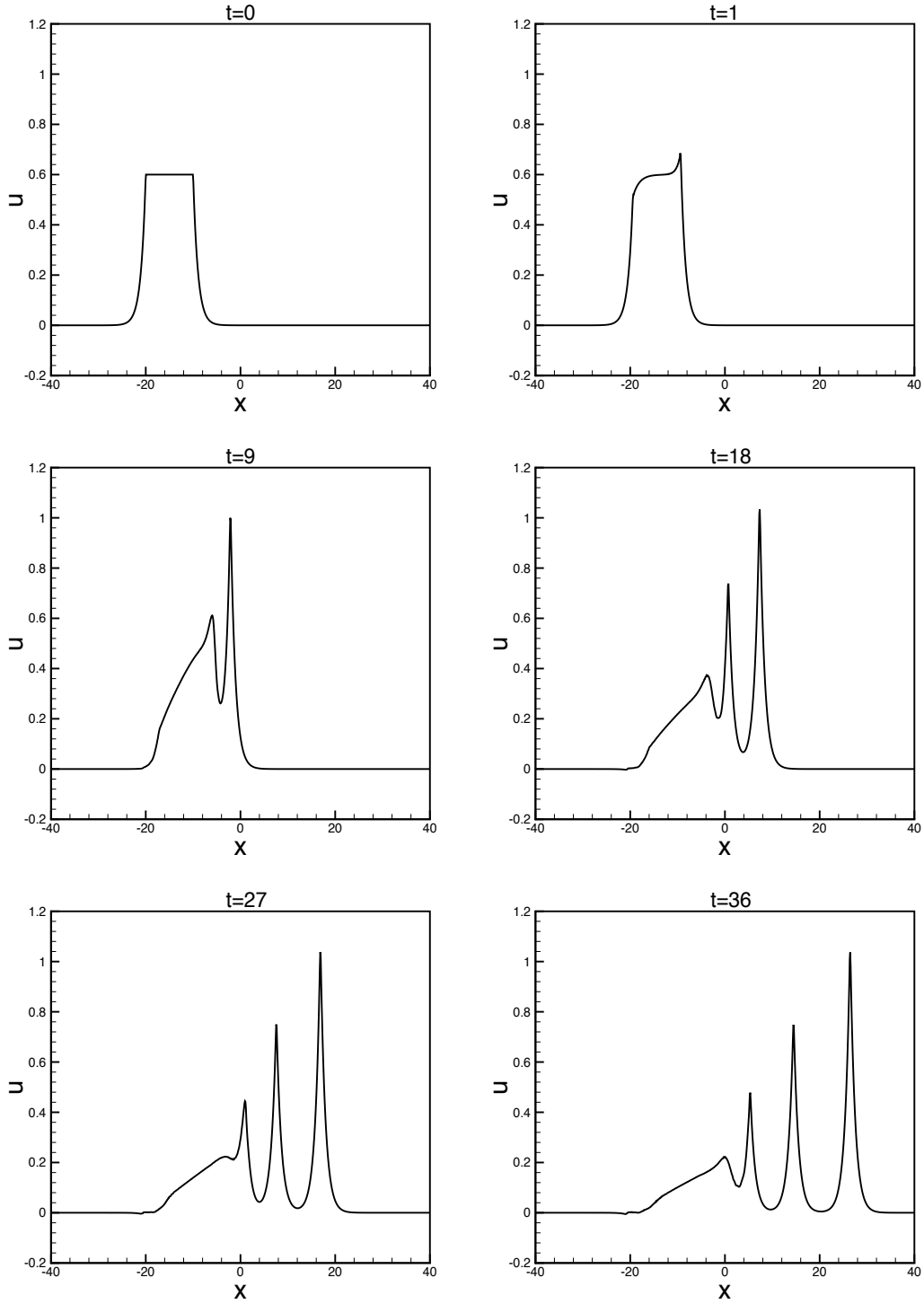
Figure 5.5: The break up of plateau traveling wave of the CH equation (5.1) with the initial condition (5.11). Periodic boundary condition in $[-40, 40]$. $P^2$ elements and a uniform mesh with $N = 800$ cells.

By the same argument as that used for the $L^2$ stability in Proposition 3.1, the first term of the right hand side in (A.1) becomes

$$\mathcal{B}_j(s,\xi,v,\sigma;-s,\sigma_t,s,-\sigma,v) = \int_{I_j}(s_ts + \sigma_t\sigma)dx + \Psi_{j+\frac{1}{2}} - \Psi_{j-\frac{1}{2}}, \qquad (A.2)$$

where $\Psi = v^-s^- - \widehat{v}s^- - \widetilde{s}v^- + \sigma_t^-s^- - \widehat{\sigma}_ts^- - \widehat{s}\sigma_t^-$.

As to the second term of the right hand side in (A.1), we have

$$\mathcal{B}_j(s^e,\xi^e,v^e,\sigma^e;-s,\sigma_t,s,-\sigma,v)$$
$$= \int_{I_j}(s_t^es + \sigma^e\sigma_t)dx + \int_{I_j}(\sigma^ev - v^e\sigma)dx + \int_{I_j}(\sigma_t^es_x + s^e(\sigma_t)_x + v^es_x + s^ev_x)dx \qquad (A.3)$$
$$+ ((\widehat{v^e} + \widehat{\sigma_t^e})[s])_{j-\frac{1}{2}} + (\widehat{s^e}[\sigma_t])_{j-\frac{1}{2}} + (\widetilde{s^e}[v])_{j-\frac{1}{2}} + \Phi_{j+\frac{1}{2}} - \Phi_{j-\frac{1}{2}},$$

where $\Phi = -\widehat{v^e}s^- - \widetilde{s^e}v^- - \widehat{\sigma_t^e}s^- - \widehat{s^e}\sigma_t^-$. Because $\mathcal{P}$ is a local $L^2$ projection, and $\mathcal{P}^+$, even though not a local $L^2$ projection, does have the property that $s - \mathcal{P}^+s$ is locally orthogonal to all polynomials of degree up to $k-1$, we have

$$\int_{I_j}\sigma^e\sigma_tdx + \int_{I_j}(\sigma^ev - v^e\sigma)dx + \int_{I_j}(\sigma_t^es_x + s^e(\sigma_t)_x + v^es_x + s^ev_x)dx = 0.$$

Noticing the special interpolating property of the projection $\mathcal{P}^-$, we also have

$$(\widehat{s^e}[\sigma_t])_{j-\frac{1}{2}} + (\widetilde{s^e}[v])_{j-\frac{1}{2}} = 0.$$

The equation (A.3) then becomes

$$\mathcal{B}_j(s^e,\xi^e,v^e,\sigma^e;-s,\sigma_t,s,-\sigma,v) = \int_{I_j}s_t^esdx + ((\widehat{v^e} + \widehat{\sigma_t^e})[s])_{j-\frac{1}{2}} + \Phi_{j+\frac{1}{2}} - \Phi_{j-\frac{1}{2}},$$

Combining the above equation with (A.2), summing over $j$ and taking into account the periodic boundary condition, we obtain the desired equality (4.17).

## A.2   Proof of Lemma 4.6

The proof of Lemma 4.6 is similar to that of Lemma 3.5 in [31]. The main difference is that we take $\bar{r}_h = \frac{1}{2}(r_h^+ + r_h^-)$, $u_h^+$ and $r_h^-$ as the reference values of the functions $r_h$ and $u_h$ at each boundary point. For the nonlinear terms $b(r)u$ and $B(r)$, we use the following Taylor expansions

$$B(r) - B(r_h) = b(r)\sigma - \frac{1}{2}b'(r)\sigma^2 - b(r)\sigma^e + b'(r)\sigma\sigma^e - \frac{1}{2}b'(r)(\sigma^e)^2,$$
$$B(r) - B(r_h^-) = b(r)\sigma^- - \frac{1}{2}b'(r)(\sigma^-)^2 - b(r)(\sigma^e)^- + b'(r)\sigma^-(\sigma^e)^- - \frac{1}{2}b'(r)((\sigma^e)^-)^2,$$

where we use the property $B'(r) = b(r)$ and $b^{(m)}(r) = 0, \quad m \geq 2$.

$$b(r)u - b(r_h)u_h$$

$$=b'(r)u\sigma + b(r)s - b'(r)s\sigma - b'(r)u\sigma^e - b(r)s^e + b'(r)s\sigma^e + b'(r)\sigma s^e - b'(r)\sigma^e s^e,$$

$$b(r)u - \widehat{b}(r_h)u_h^+$$

$$=b'(r)u\bar{\sigma} + b(r)s^+ - b'(r)\bar{\sigma}s^+ - b'(r)u\bar{\sigma}^e - b(r)(s^e)^+$$

$$+ b'(r)s^+\bar{\sigma}^e + b'(r)\bar{\sigma}(s^e)^+ - b'(r)\bar{\sigma}^e(s^e)^+.$$

These imply the following representation

$$\sum_{j=1}^{N} \mathbf{R}_j(b, B; r, u, r_h, u_h; s, -\sigma) = \mathcal{S}_1 + \mathcal{S}_2 + \mathcal{S}_3 + \mathcal{S}_4 + \mathcal{S}_5, \tag{A.4}$$

where

$$\mathcal{S}_1 = \sum_{j=1}^{N} \int_{I_j} b'(r)u\sigma\sigma_x dx + \sum_{j=1}^{N} (b'(r)u\bar{\sigma}[\sigma])_{j+\frac{1}{2}}$$

$$+ \sum_{j=1}^{N} \int_{I_j} b(r)(s\sigma)_x dx + \sum_{j=1}^{N} (b(r)(s^+[\sigma] + \sigma^-[s]))_{j+\frac{1}{2}},$$

$$\mathcal{S}_2 = -\frac{1}{2}\left(\sum_{j=1}^{N} \int_{I_j} b'(r)(s\sigma^2)_x dx + \sum_{j=1}^{N} (b'(r)(2s^+\bar{\sigma}[\sigma] + (\sigma^-)^2[s]))_{j+\frac{1}{2}}\right),$$

$$\mathcal{S}_3 = -\sum_{j=1}^{N} \int_{I_j} b'(r)u\sigma^e\sigma_x dx - \sum_{j=1}^{N} (b'(r)u\bar{\sigma}^e[\sigma])_{j+\frac{1}{2}}$$

$$- \sum_{j=1}^{N} \int_{I_j} b(r)(\sigma^e s_x + s^e\sigma_x) dx - \sum_{j=1}^{N} (b(r)((s^e)^+[\sigma] + (\sigma^e)^-[s]))_{j+\frac{1}{2}},$$

$$\mathcal{S}_4 = \sum_{j=1}^{N} \int_{I_j} b'(r)\sigma^e(s\sigma)_x dx + \sum_{j=1}^{N} (b'(r)(s^+\bar{\sigma}^e[\sigma] + (\sigma^e)^-\sigma^-[s]))_{j+\frac{1}{2}}$$

$$+ \sum_{j=1}^{N} \int_{I_j} b'(r)s^e\sigma\sigma_x dx + \sum_{j=1}^{N} (b'(r)\bar{\sigma}(s^e)^+[\sigma])_{j+\frac{1}{2}},$$

$$\mathcal{S}_5 = -\frac{1}{2}\left(\sum_{j=1}^{N} \int_{I_j} b'(r)((\sigma^e)^2 s_x + 2\sigma^e s^e\sigma_x) dx \right.$$

$$\left. + \sum_{j=1}^{N} (b'(r)(2(s^e)^+\bar{\sigma}^e[\sigma] + ((\sigma^e)^-)^2[s]))_{j+\frac{1}{2}}\right)$$

will be estimated separately later.

- The $\mathcal{S}_1$ term.

    After a simple integration by parts, it is easy to obtain

$$\mathcal{S}_1 = -\frac{1}{2}\sum_{j=1}^{N} \int_{I_j} (b'(r)u)_x\sigma^2 dx - \sum_{j=1}^{N} \int_{I_j} (b(r))_x s\sigma dx \leq C\|\sigma\|^2 + \frac{1}{8}\|s\|^2. \tag{A.5}$$

- The $\mathcal{S}_2$ term.

  After a simple integration by parts, it is easy to obtain

  $$\mathcal{S}_2 = \frac{1}{2} \sum_{j=1}^{N} \int_{I_j} (b'(r))_x s \sigma^2 dx = 0. \tag{A.6}$$

- The $\mathcal{S}_3$ term.

  We can rewrite $\mathcal{S}_3$ into the following form

  $$\mathcal{S}_3 = - \sum_{j=1}^{N} \int_{I_j} (b'(r)u - b'(r_j)u_j) \sigma^e \sigma_x dx - \sum_{j=1}^{N} \int_{I_j} b'(r_j) u_j \sigma^e \sigma_x dx$$

  $$- \sum_{j=1}^{N} \int_{I_j} (b(r) - b(r_j))(\sigma^e s_x + s^e \sigma_x) dx - \sum_{j=1}^{N} \int_{I_j} b(r_j)(\sigma^e s_x + s^e \sigma_x) dx$$

  $$- \sum_{j=1}^{N} (b'(r)u\bar{\sigma}^e[\sigma])_{j+\frac{1}{2}} - \sum_{j=1}^{N} (b(r)(\sigma^e)^-[s])_{j+\frac{1}{2}} - \sum_{j=1}^{N} (b(r)(s^e)^+[\sigma])_{j+\frac{1}{2}}.$$

  The second term, the fourth term and the last term in the above equation are zero by the definition of the special projection. Because of $|b'(r)u - b'(r_j)u_j| = O(h)$ on each element $I_j$, then by the inverse property (i) in (4.9), together with the interpolation property (4.8), the first term in the above equation is estimated by

  $$|\sum_{j=1}^{N} \int_{I_j} (b'(r)u - b'(r_j)u_j) \sigma^e \sigma_x dx| \leq C\|\sigma^e\|\|\sigma\| \leq C\|\sigma\|^2 + Ch^{2k+2}.$$

  By the same argument we can also get the estimate for the third term

  $$|\sum_{j=1}^{N} \int_{I_j} (b(r) - b(r_j))(\sigma^e s_x + s^e \sigma_x) dx| \leq C\|\sigma\|^2 + \frac{1}{8}\|s\|^2 + Ch^{2k+2}.$$

  Now we can get the estimate of $\mathcal{S}_3$

  $$\mathcal{S}_3 \leq \sum_{j=1}^{N} (|b'(r)u\bar{\sigma}^e[\sigma]| + |b(r)(\sigma^e)^-[s]|)_{j+\frac{1}{2}} + C\|\sigma\|^2 + \frac{1}{8}\|s\|^2 + Ch^{2k+2}. \tag{A.7}$$

- $\mathcal{S}_4$ and $\mathcal{S}_5$ terms.

  Because $\mathcal{S}_4$ and $\mathcal{S}_5$ are high order terms in the Taylor expansion, it is easy to show by Young's inequality and the inverse properties (i) and (ii) in (4.9) that

  $$\mathcal{S}_4 \leq Ch^{-1}(\|\sigma^e\|_\infty + \|s^e\|_\infty)\|\sigma\|\|s\| \leq C\|\sigma\|^2 + \frac{1}{8}\|s\|^2, \tag{A.8}$$

  $$\mathcal{S}_5 \leq Ch^{-1}\|\sigma^e\|_\infty(\|\sigma^e\|\|s\| + \|s^e\|\|\sigma\|) \leq C\|\sigma\|^2 + \frac{1}{8}\|s\|^2 + Ch^{2k+2}. \tag{A.9}$$

Therefore, summing up the above estimates from equations (A.5) to (A.9), we complete the proof of Lemma 4.6.

# References

[1] R. Artebrant and H.J. Schroll, *Numerical simulation of Camassa-Holm peakons by adaptive upwinding*, Appl. Numer. Math., **56** (2006), pp.695-711.

[2] A. Bressan and A. Constantin, *Global conservative solutions of the Camassa-Holm equation*, Arch. Rat. Mech. Anal., to appear.

[3] A. Bressan and A. Constantin, *Global dissipative solutions of the Camassa-Holm equation*, preprint 2006.

[4] R. Camassa and D. Holm, *An integrable shallow water equation with peaked solitons*, Phys. Rev. Lett., **71** (1993), pp.1661-1664.

[5] R. Camassa, D. Holm and J. Hyman, *A new integrable shallow water equation*, Adv. Appl. Mech., **31** (1994), pp.1-33.

[6] P. Ciarlet, *The finite element method for elliptic problem*, North Holland, 1975.

[7] B. Cockburn, *Discontinuous Galerkin methods for methods for convection-dominated problems*, in *High-Order Methods for Computational Physics*, T.J. Barth and H. Deconinck, editors, Lecture Notes in Computational Science and Engineering, volume 9, Springer, 1999, pp.69-224.

[8] B. Cockburn and C.-W. Shu, *TVB Runge-Kutta local projection discontinuous Galerkin finite element method for conservation laws II: general framework*, Math. Comp., **52** (1989), pp.411-435.

[9] B. Cockburn and C.-W. Shu, *The local discontinuous Galerkin method for time-dependent convection-diffusion systems*, SIAM J. Numer. Anal., **35** (1998), pp.2440-2463.

[10] B. Cockburn and C.-W. Shu, *Runge-Kutta Discontinuous Galerkin methods for convection-dominated problems*, J. Sci. Comput., **16** (2001), pp.173-261.

[11] B. Cockburn and C.-W. Shu, *Foreword for the special issue on discontinuous Galerkin method*, J. Sci. Comput., **22-23** (2005), pp.1-3.

[12] C. Dawson, *Foreword for the special issue on discontinuous Galerkin method*, Comput. Meth. Appl. Mech. Engin., **195** (2006), p.3183.

[13] C. Eskilsson and S.J. Sherwin, *A discontinuous spectral element model for Boussinesq-type equations*, J. Sci. Comput., **17** (2002), pp.143-152.

[14] C. Eskilsson and S.J. Sherwin, *Discontinuous Galerkin spectral/hp element modelling of dispersive shallow water systems*, J. Sci. Comput., **22/23** (2005), pp.269-288.

[15] C. Eskilsson and S.J. Sherwin, *Spectral/hp discontinuous Galerkin methods for modelling 2D Boussinesq equations*, J. Comput. Phys., **212** (2006), pp.566-589.

[16] H. Holden and X. Raynaud, *A convergent numerical scheme for the Camassa-Holm equation based on multipeakons*, Discrete Contin. Dyn. Syst., **14** (2006), pp.505-523.

[17] H. Holden and X. Raynaud, *Convergence of a finite difference scheme for the CamassaHolm equation*, SIAM J. Numer. Anal., **44** (2006) pp.1655-1680.

[18] R.S. Johnson, *Camassa-Holm, Korteweg-de Vries and related models for water waves*, J. Fluid Mech., **455** (2002), pp.63-82.

[19] R.S. Johnson, *On solutions of the Camassa-Holm equation*, R. Soc. Lond. Proc. Ser. A Math. Phys. Eng. Sci., **459** (2003), pp.1687-1708.

[20] H. Kalisch and J. Lenells, *Numerical study of traveling-wave solutions for the Camassa-Holm equation*, Chaos Solitons Fractals, **25** (2005), pp.287-298.

[21] H. Kalisch and X. Raynaud, *Convergence of a spectral projection of the Camassa-Holm equation*, Numer. Methods Partial Differential Equations, **22** (2006), pp.1197-1215.

[22] J. Lenells, *Traveling wave solutions of the Camassa-Holm equation*, J. Differential Equations, **217** (2005), pp.393-430.

[23] J. Lenells, *Conservation laws of the Camassa-Holm equation*, J. Phys. A, **38** (2005), pp.869-880.

[24] D. Levy, C.-W. Shu and J. Yan, *Local discontinuous Galerkin methods for nonlinear dispersive equations*, J. Comput. Phys., **196** (2004), pp.751-772.

[25] Y.S. Li and J.E. Zhang, *The multiple-soliton solution of the Camassa-Holm equation*, Proc. R. Soc. Lond. Ser. A Math. Phys. Eng. Sci., **460** (2004), pp.2617-2627.

[26] C.-W. Shu and S. Osher, *Efficient implementation of essentially non-oscillatory shock-capturing schemes*, J. Comput. Phys., **77** (1988), pp.439-471.

[27] Y. Xu and C.-W. Shu, *Local discontinuous Galerkin methods for three classes of nonlinear wave equations*, J. Comput. Math., **22** (2004), pp.250-274.

[28] Y. Xu and C.-W. Shu, *Local discontinuous Galerkin methods for nonlinear Schrödinger equations*, J. Comput. Phys., **205** (2005), pp.72-97.

[29] Y. Xu and C.-W. Shu, *Local discontinuous Galerkin methods for two classes of two dimensional nonlinear wave equations*, Physica D, **208** (2005), pp.21-58.

[30] Y. Xu and C.-W. Shu, *Local discontinuous Galerkin methods for the Kuramoto-Sivashinsky equations and the Ito-type coupled KdV equations*, Comput. Meth. Appl. Mech. Engin., **195** (2006), pp.3430-3447.

[31] Y. Xu and C.-W. Shu, *Error estimates of the semi-discrete local discontinuous Galerkin method for nonlinear convection-diffusion and KdV equations*, Comput. Meth. Appl. Mech. Engin., to appear.

[32] J. Yan and C.-W. Shu, *A local discontinuous Galerkin method for KdV type equations*, SIAM J. Numer. Anal., **40** (2002), pp.769-791.

[33] J. Yan and C.-W. Shu, *Local discontinuous Galerkin methods for partial differential equations with higher order derivatives*, J. Sci. Comput., **17** (2002), pp.27-47.

[34] Q. Zhang and C.-W. Shu, *Error estimates to smooth solutions of Runge-Kutta discontinuous Galerkin methods for scalar conservation laws*, SIAM J. Numer. Anal., **42** (2004), pp.641-666.